JTCM Journal of Traditional Chinese Medicine

Online Submissions: http://www.journaltcm.com
ISSN 0255-2922
info@journaltcm.com

Original Article

High-throughput sequencing analysis of differential microRNA expression in the process of blocking the progression of chronic atrophic gastritis to gastric cancer by Xianglian Huazhuo formula (香连化浊方)

GUO Yuxi, LI Ze, CHENG Nan, JIA Xuemei, WANG Jie, MA Hongyu, ZHAO Runyuan, LI Bolin, XUE Yucong, CAI Yanru, YANG Qian

GUO Yuxi, LI Ze, CHENG Nan, JIA Xuemei, WANG Jie, LI Bolin, CAI Yanru, YANG Qian, Department of spleen and stomach diseases, First Affiliated Hospital of Hebei University of Traditional Chinese Medicine, Shijiazhuang 050000, China
MA Hongyu, Department of Traditional Chinese Medicine, Hebei General Hospital, Shijiazhuang 050051, China
ZHAO Runyuan, Department of Gastroenterology, the First Affiliated Hospital of Guangzhou University of Chinese Medicine, Guangzhou 510405, China
XUE Yucong, College of Integrative Medicine, Hebei University of Chinese Medicine, Shijiazhuang 050011, China
Supported by Construction Project of National Clinical Research Base of Traditional Chinese Medicine (Science Letter [2018] No. 131, State Office of Traditional Chinese Medicine); Natural Science Foundation of Hebei Province: Study on the Mechanism of Action of Traditional Chinese Medicine on Disease and Syndrome (No. H2023423001); Key Research Project of the Ministry of Science and Technology (No. 2018YFC1704100); Key Research Project of the Ministry of Science and Technology: Li Diangui Famous Old Chinese Medicine of Traditional Chinese Medicine Academic View Characteristic, Diagnosis and Treatment Methods and Experience of Prevention and Control of Major Diseases (No. 2018YFC1704102); Provincial Science and Technology Program of Hebei Province: Prevention and Treatment of Gastric Cancer by Blocking the "Inflammation-Cancer Transformation" Based on the Theory of Turbidimetric Toxicity (No. 21377724D); Provincial Science and Technology Program of Hebei Province: to Study the Clinical Efficacy and Mechanism of Huazhuo Jiedu Formula in the Treatment of Chronic Atrophic Gastritis based on Epidermal Growth Factor Receptor/Mitogen Activated Protein Kinase/Extracellular Signal-Regulated Kinase Signaling Pathway (No. 21377740D); Scientific Research Project of Hebei Administration of Traditional Chinese Medicine: Clinical Study of Huazhuo Jiedu Formula Blocking the Pathological Evolution of Chronic Atrophic Gastritis (No. 2022026); Scientific Research Project of Hebei Administration of Traditional Chinese Medicine: Study on the Medication Rules of Spleen and Stomach Diseases of Famous Yanzhao Medical Doctors Based on Data Mining (No. 2022032); Scientific Research Project of Hebei Administration of Traditional Chinese Medicine: to Explore the Mechanism of Xianglian Huazhuo Formula in the Treatment of Chronic Atrophic Gastritis based on Transcriptomics (No. 2023022)
Correspondence to: YANG Qian, Department of spleen and stomach diseases, First Affiliated Hospital of Hebei University of Traditional Chinese Medicine, Shijiazhuang 050000, China. yang0311qian@126.com; **CAI Yanru,** Department of spleen and stomach diseases, First Affiliated Hospital of Hebei University of Traditional Chinese Medicine, Shijiazhuang 050000, China. 137544977@qq.com

Telephone: +86-13832355120; +86-15203319182
DOI: 10.19852/j.cnki.jtcm.20240617.002
Received: March 22, 2023
Accepted: July 24, 2023
Available online: June 17, 2024

Abstract

OBJECTIVE: To explore the mechanism of Xianglian Huazhuo formula (香连化浊方, XLHZ) blocking the development of chronic atrophic gastritis (CAG) to gastric cancer (GC) through bioinformatics analysis and *in vitro*.

METHODS: Pathological morphology of gastric mucosa of rats were observed. High-throughput sequencing was used to analyze the miRNA expression profile of gastric mucosa. The miRanda, miRDB and miRWalk databases were used to predict the differential target genes. Gene Ontology (GO) and Kyoto Encyclopedia of Genes and Genomes (KEGG) enrichment analysis were performed for differential target genes. Real-time quantitative reverse transcription polymerase chain reaction (qRT-PCR) was used to verify the differentially expressed miRNAs and target genes. Western blot, EdU, wound healing and flow cytometry were used to observe the effect of XLHZ on epithelial-mesenchymal transition (EMT) markers, proliferation, migration, apoptosis and cell cycle of CAG cells *in vitro*.

RESULTS: A total of five differentially expressed miRNAs and four differential target genes were screened in this study. GO analysis showed that the target genes were enriched in regulation of neuron development, regulation of transcription factor activity and regulation of RNA polymerase. KEGG pathways database differences in gene enrichment of target genes in the Wnt signaling pathway, Phospholipase D signaling pathway and mitogen-activated protein kinase signaling pathway. qRT-PCR confirmed that miRNAs and its target genes were consistent with the screening results. *In vitro*, our study revealed that XLHZ could increase the expression of E-cadherin, decrease the expression of transforming growth factor β1, vimentin and β-catenin, inhibite the proliferation

and migration of CAG cells, cause cell cycle arrest at G0/G1 and G2/M phase, induce the apoptosis of CAG cells, and prevent the progression of CAG to GC.

CONCLUSION: This study provided a new idea for the mechanism of blocking the progression of CAG to GC by XLHZ, which may be related to the expression of miR-20a-3p, miR-320-3p, miR-34b-5p, miR-483-3p and miR-883-3p and their target genes transferrin receptor, nuclear receptor subfamily 4 member 2, delta like canonical Notch ligand 1 and a kinase anchor protein 12 in CAG. In the future, we will continue to investigate the linkage between the active ingredients of XLHZ and the relevant miRNAs and their target genes, so as to provide more sufficient experimental basis for clinically effective prevention of CAG to GC.

© 2024 JTCM. All rights reserved.

Keywords: high-throughput nucleotide sequencing; gastritis, atrophic; stomach neoplasms; microRNAs; Xianglian Huazhuo formula

1. INTRODUCTION

Chronic atrophic gastritis (CAG) is a disease of the digestive system in which multiple pathogenic factors act on the gastric mucosa, causing a decrease or even loss of the number of glands in the lamina propria of the gastric mucosa, and may be accompanied by intestinal hyperplasia and (or) pseudopyloric adenomatous hyperplasia.[1] The clinical manifestations are not obviously specific, and most of the symptoms are mainly upper abdominal pain, abdominal distension, nausea and dry vomiting. According to the widely accepted Correa model of gastric cancer (GC) development, normal gastric mucosa undergoes precancerous lesions of gastric cancer (PLGC) (intestinal epithelial metaplasia or intraepithelial neoplasia) through chronic inflammation and chronic atrophic gastritis and eventually develops into GC,[1-4] during which epithelial-mesenchymal transition (EMT) is directly triggered, thus stimulating tumor spread and metastasis.[5,6] Moreover, CAG leads to progressive development of GC due to the absence of obvious specific symptoms and painful examination mean. When GC is found, most of them have already developed to the middle and late stages, which brings great problems for the treatment and the quality of life of patients.[7] Currently, western medicine mainly focuses on symptomatic treatments such as eradication of helicobacter pylori (HP), inhibition of gastric acid secretion and protection of gastric mucosa, which are difficult to eradicate and have a high recurrence rate.[8,9] Therefore, the exploration of drugs that effectively block the progression of CAG to GC is important to reduce clinical GC mortality, improve patient survival quality, and reduce national healthcare costs. Several domestic and international studies[10-13] have shown that Traditional Chinese Medicine (TCM) embodied a broad prospect and obvious advantages in intervening in PLGC with outstanding efficacy. However, the mechanism is still unclear and needs to be further investigated.

Xianglian Huazhuo formula (香连化浊方, XLHZ) is composed of Huanglian (*Rhizoma Coptidis*), Baizhu (*Rhizoma Atractylodis Macrocephalae*), Baidoukou (*Fructus Amomi Rotundus*), Baihuasheshecao (*Herba Hedyotidis*), Danggui (*Radix Angelicae Sinensis*), Chuanxiong (*Rhizoma Chuanxiong*), Sanqi (dash) (*Radix Notoginseng*), Fuling (*Poria*), Baishao (*Radix Paeoniae Alba*), Baihe (*Bulbus Lilii Lancifolii*), Zhishi (*Fructus Aurantii Immaturus*), Xiangfu (*Rhizoma Cyperi*), Muxiang (*Radix Aucklandiae*), Quanxie (*Scorpion*), Yanhusuo (*Rhizoma Corydalis Yanhusuo*), Huoxiang (*Herba Agastaches Rugosa*), Sharen (*Fructus Amomi*), Banzhilian (*Herba Scutellariae Barbatae*). It is soured from the classical Chinese medicine prescriptions "Ganluxiaodu Dan (甘露消毒丹), Xiaoyao San (逍遥散) and Chaihushugan San (柴胡疏肝散)", and is improved from the clinical practice of Professor LI Diangui, a national medical master of Hebei Provincial Hospital of Traditional Chinese Medicine. Based on our current research findings, XLHZ could effectively improve the pathological damage of CAG gastric mucosa by participating in biological processes such as cell proliferation, apoptosis and inflammatory response, and regulating PI3K/Akt and MAPK signaling pathways.[14-16] MicroRNA (miRNA), a non-coding RNA with a length of about 19-25 and nucleotides, has a negative regulatory effect on mRNA in tumor cells.[17] Several studies have shown that miRNA played an important role in the early diagnosis, treatment and prognostic assessment of GC.[18-20] Therefore, in the present study, we performed bioinformatics analysis of miRNA expression profiles by high-throughput sequencing technology to explore the possible mechanism of XLHZ in the treatment of CAG and to provide new ideas for intercepting the progression of CAG to GC.

2. MATERIALS AND METHODS

2.1. Drugs

XLHZ [Huanglian (*Rhizoma Coptidis*) 6 g, Baizhu (*Rhizoma Atractylodis Macrocephalae*) 12 g, Baidoukou (*Fructus Amomi Rotundus*) 6 g, Baihuasheshecao (*Herba Hedyotidis*) 15 g, Danggui (*Radix Angelicae Sinensis*) 12 g, Chuanxiong (*Rhizoma Chuanxiong*) 9 g, Sanqi (dash) (*Radix Notoginseng*) 2 g, Fuling (*Poria*) 15 g, Baishao (*Radix Paeoniae Alba*) 15 g, Baihe (*Bulbus Lilii Lancifolii*) 12 g, Zhishi (*Fructus Aurantii Immaturus*) 10 g, Xiangfu (*Rhizoma Cyperi*) 9 g, Muxiang (*Radix Aucklandiae*) 6 g, Quanxie (*Scorpion*) 3 g, Yanhusuo (*Rhizoma Corydalis Yanhusuo*) 10 g, Huoxiang (*Herba Agastaches Rugosa*) 10 g, Sharen (*Fructus Amomi*) 6 g, Banzhilian (*Herba Scutellariae Barbatae*) 15 g] was provided by the pharmacy of Hebei Provincial Hospital of Traditional Chinese Medicine, and concentrated into a liquid containing 3.6 g/mL of raw herbs, the drug was administered once daily for 60 d. Sodium salicylate (Tianjin Baishi Chemical Co., Ltd., Tianjin, China, Lot No. 20210302). N-Methyl-N'-Nitro-N-Nitrosoguanidine (MNNG) (Shanghai Aladdin Biochemical Technology Co., Ltd., Shanghai, China, Lot No. M105583).

2.2. Ethics statement and animal handing

This animal experiment was approved by the Animal Ethics Committee of Hebei College of Traditional Chinese Medicine, with the approval number: DWLL2019022.

Thirty specific pathogen free (SPF)-grade male Wistar rats [aged 6-8 weeks, weight (150 ± 20) g], were purchased from Beijing Viton Lihua Laboratory Animal Technology Co., Ltd. (Beijing, China, [Certificate No. SCXK (Beijing) 2016-0006]). The rats were housed in the SPF-class laboratory animal center of Hebei College of Traditional Chinese Medicine, fed with common chow, and fed and watered ad libitum. Reference[39] was used to prepare the CAG rat model by the composite moulding method. (a) MNNG, solution 180 μg/mL was drunk freely from the light and changed daily; (b) 2% sodium salicylate 1 mL/100 g was gavaged when rats were hungry; (c) hunger and satiety disorders: rats were given 2 d of adequate food and 1 d of fasting alternately.

A total of thirty rats were divided into three groups with 10 rats in each group by table of random numbers: (a) normal, (b) model (MNNG, 180 μg/mL + 2% sodium salicylate, 1 mL/100 g per day + hunger and satiety disorders), (c) XLHZ (model + XLHZ, 36 $g \cdot kg^{-1} \cdot d^{-1}$), which was calculated according to the equivalent dosage table of human and rat body surface area. After the last gavage, the rats were fasted without water for 24 h, anesthetized, and the stomach tissues were isolated by rapid opening of the abdominal cavity, part of which was stored in a freezing tube in a liquid nitrogen tank and quickly transferred to —80℃ refrigerator for storage; part of which was stored in 4% paraformaldehyde for hematoxylin-eosin (HE) staining and pathological histological evaluation.

2.3. Histological examination

The fixed gastric tissues were taken, paraffin-embedded, sectioned (4 μm thick), HE stained and sealed with neutral gum. The histopathological structural changes of the rat gastric mucosa were observed under the microscope.

2.4. miRNA sequencing and analysis

Total RNA was isolated using miRNeasy Mini Kit (50) 217004 (Qiagen, Dusseldorf, Germany), after which the RNA concentration and quality were determined by the Qubit®2.0 Fluorometer (Thermo Fisher Scientific Inc., Waltham, MA, USA) and the Nanodrop One spectrophotometer (Thermo Fisher Scientific Inc., Waltham, MA, USA). Integrity of total RNA was assessed using the Agilent 2100 Bioanalyzer (Agilent Technologies Inc., Palo Alto, CA, USA), and samples with RNA integrity number (RIN) values above 7.0 were used for sequencing.

The synthesis of the paired-end library was done strictly according to the QIAseq miRNA library kit guidelines. Real -time quantitative reverse transcription polymerase chain reaction (qRT-PCR) was performed to purify and enrich the products to form the final cDNA library. The purified libraries were quantified using a Qubit® 2.0 fluorometer, validated using a Gitzo 2100 Bioanalyzer (Agilent Technologies Inc., Palo Alto, CA, USA) to determine the size of the insert and calculate the molar concentration. Clustering was generated with cBot, libraries were diluted to 10 pM, and then sequenced on an Illumina Hiseq Xten (Illumina, San Diego, CA, USA). The miRNAs were subjected to differential expression analysis applying DESeq software. With |log2(FC)| value > 1 and P value < 0.05 was considered statistically significant for the next analysis.

2.5. Bioinformatics analysis

The miRanda, miRDB and miRWalk databases were applied to predict the target genes of the differentially expressed miRNAs. The predicted target genes were analyzed using DESeq software. Classification of the biological functions of differentially expressed miRNAs using GO. KEGG database was analyzed for the major biochemical pathways and signaling pathways involved in the target genes, with a focus on significantly enriched pathways.

2.6. qRT-PCR validation of differential miRNAs and mRNAs

Total RNA was extracted from rats gastric tissue with TRIzol reagent, reverse transcribed to cDNA and added to the amplification reaction system under the following reaction conditions: 25 ℃ for 5 min, 42 ℃ for 15 min, 85 ℃ for 5 min and maintained at 4 ℃. Subsequently, Real-time PCR assay was performed, and the reaction conditions were: pre-denaturation 95 ℃ for 15 min, followed by 40 cycles of reaction: 95 ℃ for 30 s, 95 ℃ for 15 s, 60 ℃ for 30 s. With U6 as internal reference, and the relative expression was calculated by the $2^{-\Delta\Delta CT}$ method according to the relative quantitative analysis. All experiments were performed three times independently. For qRT-PCR, sequence-specific primers were as follows: miR-20a-3p: F-5'-ACACTCCAGCTGGGACTGCATTACGAGCATGTAAGTG-3', R-5'-TGGTGT-CGTGGAGTCG-3'; miR-320-3p: F-5'-ACACTCC-AGCTGGGAAAAGCTGGGTTGAGA-3', R-5'-TGG-TGTCGTGGAGTCG-3'; miR-34b-5p: F-5'-ACACTC-CAGCTGGGAGGCAGTGTAATTAG-3', R-5'-TGG-TGTCGTGGAGTCG-3'; miR-483-3p: F-5'-ACACTC-CAGCTGGGCACTCCTCCCCTCCCG-3', R-5'-TGG-TGTCGTGGAGTCG-3'; miR-883-3p: F-5'-ACACT-CCGCTGGGTAACTGCAACATCT-3', R-5'-TGGTG-TCGTGGAGTCG-3'; Akap12: F-5'-GCGGGAGTAG-AAGAGCCAC-3', R-5'-AAGTCCACGCGCAACTC-ATA-3'; DLL1: F-5'-GTGTAAGAT-GGAGCGATG-TGGCA-3', R-5'-GGCAGTTGTGTTTCTAGTTCA-AGGAAAG-3'; NR4A2: F-5'-AGATTCCTGGCTTT-GCTGAC-3', R-5'-CTGGGTTGGACCTGTATGCT-3'; TFRC: F-5'-GGCTACTTGGGCTATTGTAAAGG-3', R-5'-CAGTTTCTCCGACAACTTTCTCT-3'.

2.7. Cell culture

Human gastric mucosal epithelial cells (GES-1) cells were resuscitated in ultra-clean bench and cultured in roswell park memorial institut (RPMI) Medium 1640 medium containing 10% fetal bovine serum (FBS) at 37 ℃ with 5% CO_2 in an incubator. The log phase GES-1 cells were inoculated in 6-well plates (1×10^6/well), and after 24 h of culture, the old medium was aspirated and discarded, 1 mL of phosphate buffered saline (PBS) was added twice to wash, and 2 mL of 10% FBS RPMI Medium 1640 medium containing 40 μM MNNG was added to induce into MNNG-induced GES-1 cells.

2.8. Preparation of drug-containing serum

XLHZ 36 $g \cdot kg^{-1} \cdot d^{-1}$ was given to rats, and blood was taken from the head after one week of continuous gavage. The blood was centrifuged at 3500 r/min for 15 min, and the upper layer of serum was set aside, inactivated in a water bath at 56 ℃ for 30 min, filtered through 0.22 μm microporous membrane to remove bacteria, and stored at －80 ℃ in an ultra-low temperature refrigerator for subsequent experiments.

2.9. Methyl thiazolyl tetrazolium (MTT) method

MNNG-induced GES-1 cells were seeded at 100 μL per well in 96-well plates and incubated at 37 ℃ overnight. The original culture medium was changed to 0%, 2.5%, 5%, 10%, 20% and 40% drug-containing serum. After incubation at 37 ℃ for 48 h, 10 μL of 5 mg/mL MTT solution were added to each well, and the incubation was continued for 4 h. 100 μL of formazan solution were added to each well, mixed, and incubated again in the cell incubator. The formazan was completely dissolved.
The optical density (OD) value of each pore was detected by microplate reader (Beijing PRong New Technology Co., Ltd., Beijing, China, No. DNM-9602) at 570 nm wavelength. The half maximal inhibitory concentration (IC50) of XLHZ on MNNG-induced GES-1 cells was calculated, and the optimal concentration of serum containing XLHZ on cell was selected.

2.10. EdU staining to detect cell proliferation

BeyoClick™ EdU-488 Cell Proliferation Assay Kit (Shanghai Beyontian Biotechnology Co., Ltd., Shanghai, China, Item No. C0071S) was used to detect cell proliferation and to detect the proliferation of each group of cells after transfection. The specific steps are: collect each group of cells inoculated in a 6-well plate and culture overnight to recover to normal state. Add 20 μM of EdU solution diluted with culture solution and leave it for 2 h at 37 ℃; discard the liquid, add 1 mL of 4% paraformaldehyde and fix for 15 min; discard the liquid, wash 3 times with PBS for 3-5 min each time; discard the liquid, add 1 mL/well containing 0.5% TritonX-100 permeate and leave it for 10-15 min at room temperature; discard the liquid, wash 1-2 times with PBS for 3-5 min each time; discard the liquid. Discard the liquid, add 0.5 mL/well of Click reaction solution, and leave it at room temperature for 30 min, then wash it 3 times with PBS for 3-5 min each time; stain the nuclei with 4', 6-Diamidino-2'-phenylindole (DAPI) for 30 min, wash it twice with PBS; add DAPI to stain the nuclei, observe by fluorescence microscope and take pictures. The number of EdU-positive cells was used to express the cell proliferation ability.

2.11. Wound healing assay to detect cell migration

Log phase GES-1 cells were collected for digestion and counting, and 6-well plates were spread at 1×10^6 million per well, and each group of cells was cultured until the density was close to fusion. The cells were washed with PBS 3 times to remove the wounded down cells by wounding with a gun tip compared to a straightedge, as perpendicular to the horizontal line behind. Put into 37 ℃, 5% CO_2 incubator to continue the culture. Photographs were taken at 0 and 48 h using an inverted microscope respectively and the wound healing rate was calculated. Wound healing rate = (0 h wound width – 12 h wound width) / 0 h wound width × 100%, and the wound healing rate indicates the cell migration ability.

2.12. Flow cytometry to detect apoptosis and cell cycle

The cells of each group were collected at 1×10^6 million per well and inoculated in 6-well plates, digested with 0.25% trypsin, 5×10^4-10^5 resuspended cells were taken, centrifuged at 1000 rpm for 5 min, the supernatant was discarded, and 500 μL of Binding Buffer (1 ×) was added to resuspend the cells; 5 μL of Annexin V-FITC and 10 μL of PI were added and mixed, and incubated at room temperature Incubate for 10-20 min at room temperature, then place in an ice bath. Cells were resuspended 2-3 times during incubation to improve the staining effect, and apoptosis rate and cell cycle were detected by flow cytometry.

2.13. Western blotting

After the drug treatment, the cells of each group were collected, and radio-immunoprecipitation assay was used to split the cells and extract the total protein. Sodium dodecyl sulfate polyacrylamide gel electrophoresis glue was prepared according to the molecular weight of the protein, and the protein was transferred from the gel to the polyvinylidene fluoride membrane to form imprinting. Use the sealing film in 5% skim milk powder at room temperature for 2 h, and incubate at 4 ℃ for primary antibody overnight. At room temperature after incubation for 1 h, bands were detected by gel imaging analysis system.

2.14. Statistical analysis

SPSS 21.0 (IBM Corp., Armonk, NY, USA) was applied to analyze the data. Statistical analyses were measured using one-way analysis of variance (ANOVA) followed by post hoc Bonferroni correction for multiple

comparisons. The results were statistically described using mean ± standard deviation, with $P < 0.05$ indicating statistical significance.

3. RESULTS

3.1. Histologic changes in the gastric mucosal tissue

Hematoxylin and eosin (HE) staining results (Figure 1) revealed a decrease in epithelium in the model group. The arrangement of glands in the lamina propria was disordered and atrophied, the number was reduced, the atrophy of glands was obvious, the mucosal layer was thinned, there were a large number of lymphocytes and plasma cells and other inflammatory cells infiltrated, and congestion and edema were obvious, which was consistent with the pathological diagnosis of CAG. Compared with the model group, the mucosal layer of the XLHZ group was thickened to different degrees, the epithelial cells were still arranged, the degree of atrophy of the intrinsic glands and the amount of inflammatory cells were improved to different degrees, and the congestion and edema were significantly ameliorated.

3.2. Effect of XLHZ on miRNA expression profile of CAG

We analyzed the miRNA expression profiles of gastric mucosa tissue of rats between the normal and the model, and between the model and the XLHZ. In supplementary Table 1, Sixteen miRNAs differentially expressed [|log2, (FC)| value > 1, P value < 0.05] between the normal and the model groups, of which seven miRNAs were up-regulated and nine miRNAs were down-regulated (supplementary Figures 1A1, B1). In supplementary Table 2, Seventeen miRNAs differentially expressed [|log2 (FC)| value > 1, P value < 0.05] between the model and the XLHZ groups, of which five miRNAs were up-regulated and twelve miRNAs were down-regulated (supplementary Figures 1A2, B2). These results suggested that XLHZ could alter the miRNA expression profile of CAG rat tissues, which may be the key factors of XLHZ in the treatment of CAG.

3.3. GO and KEGG pathway enrichment analysis

The miRanda, miRDB and miRWalk databases predicted a total of 262 target genes for sixteen differentially expressed miRNAs between the normal and the model groups and 245 target genes for seventeen differentially expressed miRNAs between the model and the XLHZ groups (supplementary Figure 2). To predict the functions of the differentially expressed miRNAs, we classified the biological process, cellular components and molecular functions of the candidate target genes using GO functional annotation (supplementary Figures 3A1, 3A2). Among them, the crossover functions include positive regulation of neuron projection development and neuron differentiation, axon part, synaptic membrane, transcriptional activator activity, RNA polymerase Ⅱ core promoter proximal region sequence-specific binding, transcriptional activator activity, RNA polymerase Ⅱ transcription regulatory region sequence−specific binding, cell adhesion molecule binding and cadherin binding. The signaling pathways controlled by the differentially expressed miRNAs candidate target genes were analyzed using the Kyoto Encyclopedia of Genes and Genomes (KEGG) pathway (supplementary Figure 3B1, 3B2), and the crossover signaling pathways were found to include Wnt signaling pathway, Endocytosis, Phospholipase D signaling pathway, MAPK signaling pathway, Phosphatidylinositol signaling system, Autophagy-animal, Proteoglycans in cancer.

3.4. qRT-PCR validation of miRNAs expression

To verify the sequencing results, we performed qRT-PCR to validate the expression of five miRNAs. As shown in Table 1, the expression of miR-483-3p showed upregulated in the XLHZ group compared with the model group but were not statistically significant ($P > 0.05$). The expression of miR-20a-3p was markedly increased, while the expression of miR-320-3p, miR-34b-5p and miR-883-3p were decreased in the model group relative to the normal group ($P < 0.01$). The expression of miR-20a-3p, miR-320-3p, miR-34b-5p and miR-883-3p after treatment with XLHZ was consistent with the sequencing results. This indicated that XLHZ could achieve the effect of blocking the progression of CAG to GC by adjusting the miRNA expression profile.

3.5. Regulatory network construction and analysis

Target genes prediction was performed using miRanda, miRDB and miRWalk databases for miR-20-3p, miR-320-3p, miR-34b-5p, miR-883-3p. A total of 64 target genes were identified. As shown in supplementary

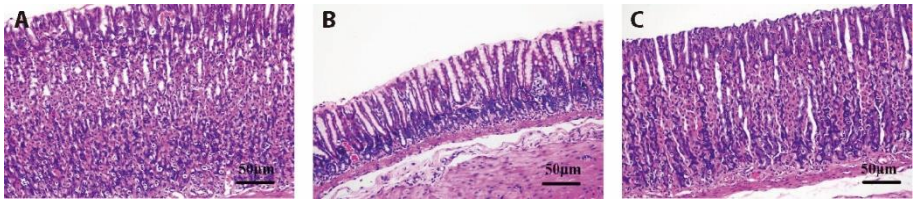

Figure 1 Histologic changes in the gastric mucosal tissue (magnification × 200, scale bar 50 μm)
A: normal group; B: model group; C: XLHZ group. normal group: drink and eat freely + the same volume of normal saline was given by gavage; model group: MNNG, 180 μg/mL + 2% sodium salicylate, 1 mL/100 g per day + hunger and satiety disorders; XLHZ: model group + XLHZ, 36 $g \cdot kg^{-1} \cdot d^{-1}$. HE: hematoxylin and eosin; CAG: chronic atrophic gastritis; XLHZ: Xianglian Huazhuo formula.

Figure 4, miRNAs and their corresponding target gene networks were displayed. The network diagram showed that miR-320-3p and miR-883-3p shared a common target gene Gmfb, miR-20a-3p and miR-883-3p shared a common target gene NR4A2. It suggested that they may have synergistic effects in some functions.

3.6. qRT-PCR validation of mRNAs expression of target genes

To further validate the predicted results, we performed qRT-PCR on the mRNA expression of the four target genes. As shown in Table 1, the level of TFRC and NR4A2 memorably increased, the level of DLL1 and Akap12 memorably decreased in the model group contrast to the normal group ($P < 0.01$). The XLHZ group revered this result ($P < 0.01$).

3.7. Screening of the optimal concentration of drug-containing serum

In supplementary Figure 5, the IC50 of XLHZ on MNNG-induced GES-1 cells was 10.02%, so 10% drug-containing serum was selected for subsequent experiments.

3.8. Effect of XLHZ on proliferation and migration of MNNG-induced GES-1 cells

As shown in Figures 2A-2B, we found that the cell proliferation rate was significantly increased in the model group. In contrast, the cell proliferation rate was remarkably decreased after XLHZ treatment. To evaluate the effect of XLHZ on migration ability of MNNG-induced GES-1 cells, we performed wound healing experiment. In Figures 2C-2D, wound healing assay confirmed that migration ability of MNNG-induced GES-1 cells was up-regulated but inhibited after XLHZ treated.

3.9. Effect of XLHZ on cell cycle and apoptosis of MNNG-induced GES-1 cells

In Figure 3A, flow cytometry results showed that compared with the normal group, the proportion of Q2 and Q3 in the model group was down-regulated ($P < 0.01$). Compared with the model group, the proportion of Q2 and Q3 in the XLHZ group was obviously up-regulated ($P < 0.01$). Thus, XLHZ could induce apoptosis of MNNG-induced GES-1 cells. Figure 3B showed the cell cycle changes before and after treatment. Compared with the normal group, G0/G1 phase cells in the model group were significantly reduced ($P < 0.01$). S phase cells in the model group were significantly increased ($P < 0.01$). The trend has reversed after intervention of XLHZ.

3.10. Effect of XLHZ on EMT of MNNG-induced GES-1 cells

The changes of EMT proteins level in rat were detected using western blotting. In Figure 4, the expression of E-cadherin was down-regulated, TGF-β1, Vimentin and β-catenin were up-regulated obviously in the model group compared to the normal group ($P < 0.01$). However, after treatment of XLHZ formula, the result was reversed.

4. DISCUSSION

The normal gastric mucosa can progress from chronic inflammation to CAG, with PLGC (intestinal epithelial metaplasia or intraepithelial neoplasia) and eventually to GC, which is the Correa gastric cancer development model widely recognized by the academic community.[1-4] Early intervention, active and effective interruption and reversal of CAG development are very beneficial in reducing the incidence of GC and improving the prognosis of patients.[21] Several clinical studies have shown that TCM embodies broad prospects and obvious advantages in intervening in CAG precancerous lesions, with outstanding efficacy, multi-targeting and low toxic side effects.[22-24] In our study, we used MNNG compound modeling method to establish a CAG model in rats to explore the mechanism of XLHZ formula in interrupting the development of CAG to GC. *In vitro*, our study have found that XLHZ may play a role by regulating the expression of miRNA to inhibit EMT, inhibit cell proliferation and migration, and promote cell apoptosis. MNNG is a carcinogen that mimics the conversion of nitrate to ammonium nitrite, which can mutate the alkylation of bases on the DNA strand and

Table 1 qRT-PCR validation of miRNAs expression

Group	*n*	Normal	Model	XLHZ
miR-20a-3p	3	1.08±0.49	6.65±1.38[a]	3.31±0.76[b]
miR-320-3p	3	1.04±0.31	0.15±0.06[a]	0.44±0.15[b]
miR-34b-5p	3	1.05±0.37	0.11±0.07[a]	0.58±0.13[c]
miR-483-3p	3	1.01±0.15	0.29±0.16[a]	0.37±0.12
miR-883-3p	3	1.03±0.28	0.21±0.05[a]	0.52±0.17[b]
Akap12	3	1.03±0.25	0.19±0.13[a]	0.76±0.25[b]
DLL1	3	1.00±0.11	0.32±0.07[a]	0.58±0.06[b]
NR4A2	3	1.06±0.40	3.28±0.50[a]	2.25±0.49[b]
TFRC	3	1.01±0.18	2.13±0.29[a]	1.64±0.22[b]

Notes: normal group: drink and eat freely + the same volume of normal saline was given by gavage; model group: MNNG, 180 μg/mL + 2% sodium salicylate, 1 mL/100 g per day + hunger and satiety disorders; XLHZ: model group + XLHZ, 36 $g \cdot kg^{-1} \cdot d^{-1}$. qRT-PCR: real-time quantitative reverse transcription polymerase chain reaction; XLHZ: Xianglian Huazhuo formula; CAG: chronic atrophic gastritis; GC: gastric cancer. Statistical analyses were measured using one-way analysis of variance followed by post hoc Bonferroni correction for multiple comparisons. Data were presented as mean ± standard deviation. Compared with the normal group, [a]$P < 0.01$; Compared with the model group, [b]$P < 0.01$, [c]$P < 0.05$.

cause cancer.[25] Sodium salicylate is a kind of non-steroidal anti-inflammatory drugs, which can inhibit the synthesis of prostaglandins and reduce the protective effect of prostaglandins. As a weak acid, it can interact with the phospholipid bilayer on the surface of mucosal cells to reduce the hydrophobicity of gastric and duodenal mucosa, thereby exposing gastric acid and other mucosal erosion factors. In addition, it can release a large number of pro-inflammatory factors and accelerate mucosal inflammation.[26] Therefore, MNNG and sodium salicy-late have been widely used to induce CAG models. Our results showed that compared with the normal group, the gastric lamina propria glands in the model group were arranged disorderly and atrophic, the number was reduced. The mucosal layer became thinner. There were a large number of lymphocytes, plasma cells and other inflammatory cells infiltrated, and congestion and edema were obvious, which indicated that we successfully induced the CAG model. High-throughput sequencing results showed that the expression of miRNA in rats induced by the compound modeling method changed. Previous studies have found that studies showed that miRNA regulates the expression of more than 1/3 of coding genes and signaling pathways *in vivo*, positively or negatively regulating processes such as repression and activation, transcriptional cleavage and enhancement, thus influencing the formation of secondary small interfering RNAs and forming a complex mRNA-mRNA network *in vivo* that is involved in the development of various tumors.[27,28] The expression of some miRNAs and their target genes were reversed after treatment of XLHZ. Therefore, we speculate that XLHZ interrupt the progression of CAG to GC by regulating miRNAs and their target genes.

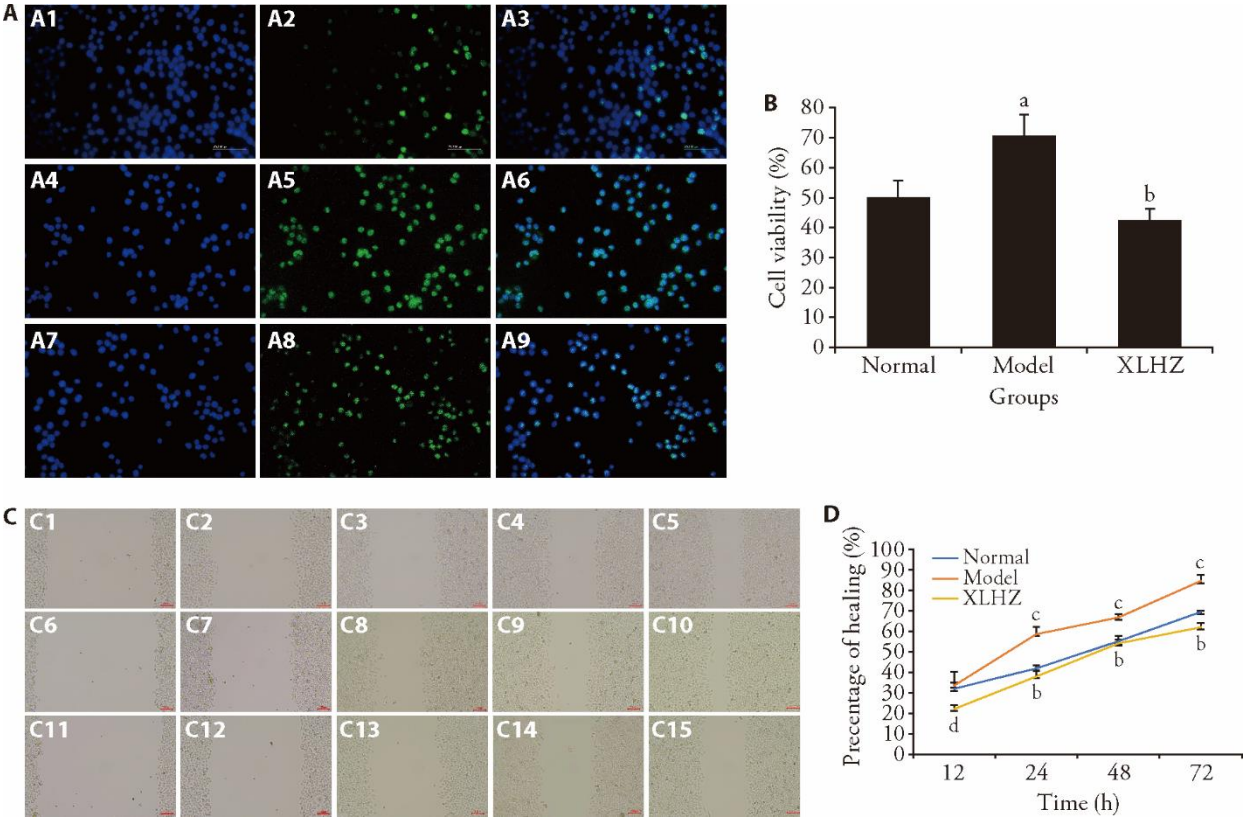

Figure 2 Effect of XLHZ on proliferation and migration of MNNG-induced GES-1 cells

A: EdU assay was used to detect cell proliferation (magnification × 200). The proliferating cells were fluorescently stained with EdU (Green). The nuclei were stained with DAPI (Blue). the higher the cell proliferation rate, the brighter the green in the plot. A1: EdU of the control group; A2: DAPI of the control group; A3: merge of the control group; A4: EdU of the model group; A5: DAPI of the model group; A6: merge of the model group; A7: EdU of the XLHZ group; A8: DAPI of the XLHZ group; A9: merge of the XLHZ group. B: Quantitative analysis of proliferating cells. C: Wound healing assay was used to detect cell migration in the normal, model and XLHZ groups (magnification × 200). C1-C5: The migration of cells in the normal group was observed at 0, 12, 24, 48, 72 h. C6-C10: The migration of cells in the model group was observed at 0, 12, 24, 48, 72 h. C11-C15: The migration of cells in the XLHZ group was observed at 0, 12, 24, 48, 72 h. D: quantitative analysis of cells migration rate at 0, 12, 24, 48, 72 h. normal group: drink and eat freely + the same volume of normal saline was given by gavage; model group: MNNG, 180 μg/mL + 2% sodium salicylate, 1 mL/100 g per day + hunger and satiety disorders; XLHZ: model group + XLHZ, 36 $g \cdot kg^{-1} \cdot d^{-1}$. XLHZ: Xianglian Huazhuo formula; MNNG: N-Methyl-N'-Nitro-N-Nitrosoguanidine; GES-1: human gastric mucosal epithelial cells; EdU: 5-Ethynyl-2'- deoxyuridine; DAPI: 4',6-Diamidino-2'-phenylindole. Statistical analyses were measured using one-way analysis of variance followed by post hoc Bonferroni correction for multiple comparisons. Data were presented as mean ± standard deviation (n = 3). Compared with the normal group, $^{a}P < 0.05$, $^{b}P < 0.01$; Compared with the model group, $^{c}P < 0.05$; $^{d}P < 0.01$.

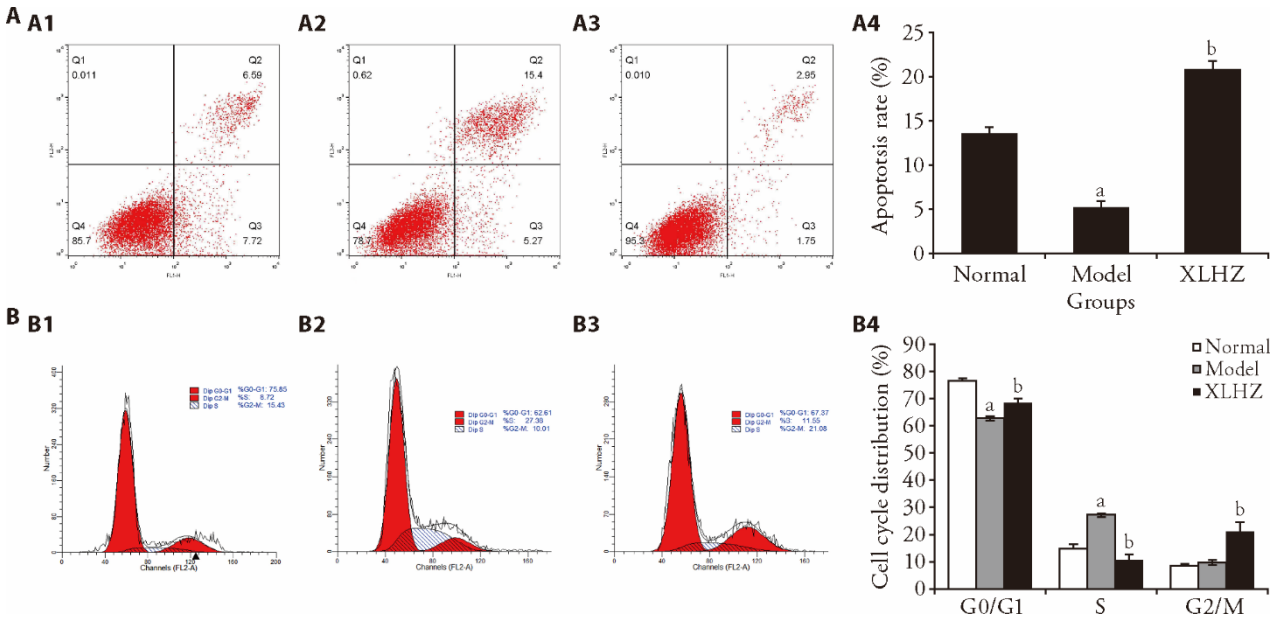

Figure 3 Effect of XLHZ on apoptosis and cell cycle of MNNG-induced GES-1 cells

A: flow cytometry assay was used to detect apoptosis in the normal, model and XLHZ groups. A1: normal group; A2: model group; A3: XLHZ group; A4: apoptosis rate of quantitative analysis. B: flow cytometry assay was used to detect cell cycle in the normal, model and XLHZ groups. B1: normal group; B2: model group; B3: XLHA group; B4: quantitative analysis of cell cycle distribution. normal group: drink and eat freely + the same volume of normal saline was given by gavage; model group: MNNG, 180 μg/mL + 2% sodium salicylate, 1 mL/100 g per day + hunger and satiety disorders; XLHZ: model group + XLHZ, 36 $g \cdot kg^{-1} \cdot d^{-1}$. XLHZ: Xianglian Huazhuo formula; MNNG: N-Methyl-N'-Nitro-N-Nitrosoguanidine; GES-1: human gastric mucosal epithelial cells. Statistical analyses were measured using one-way analysis of variance followed by post hoc Bonferroni correction for multiple comparisons. Data were presented as mean ± standard deviation (n = 3). Compared with the normal group, $^{a}P < 0.01$; Compared with the model group, $^{b}P < 0.01$.

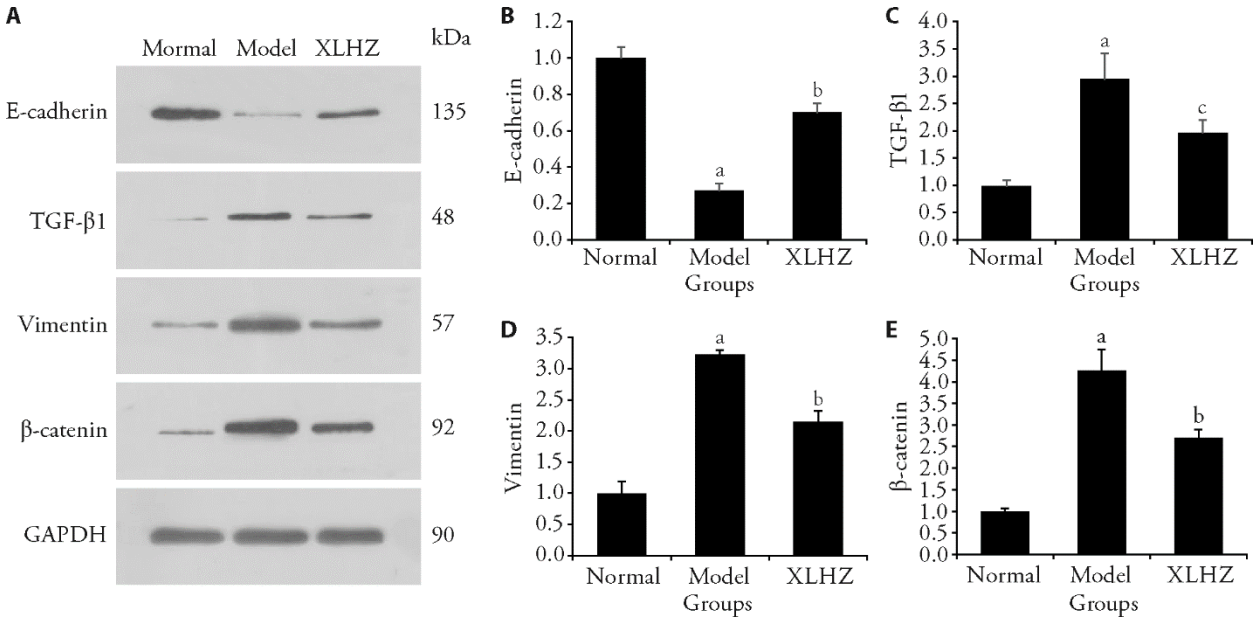

Figure 4 Effects of XLHZ on EMT and proliferation of MNNG-induced GES-1 cells

A: representative images of of E-cadherin, TGF-β1, vimentin and β-catenin protein expression that were exhibited from MNNG-induced GES-1 cells in the normal, model and XLHZ groups. B: quantitative analysis of E-cadherin protein; C: quantitative analysis of TGF-β1 protein; D: quantitative analysis of vimentin protein; E: quantitative analysis of β-catenin protein. normal group: drink and eat freely + the same volume of normal saline was given by gavage; model group: MNNG, 180 μg/mL + 2% sodium salicylate, 1 mL/100 g per day + hunger and satiety disorders; XLHZ: model group + XLHZ, 36 $g \cdot kg^{-1} \cdot d^{-1}$. XLHZ: Xianglian Huazhuo formula; EMT: epithelial mesenchymal transition; MNNG: N-Methyl-N'-Nitro-N-Nitrosoguanidine; GES-1: human gastric mucosal epithelial cells. Statistical analyses were measured using one-way analysis of variance followed by post hoc Bonferroni correction for multiple comparisons. Data were presented as mean ± standard deviation (n = 3). Compared with the normal group, $^{a}P < 0.01$; Compared with the model group, $^{b}P < 0.01$; $^{c}P < 0.05$.

EMT is considered to be an important mechanism for cancer cell metastasis, which makes tumor cell lose some characteristics of epithelial cell, such as intercellular adhesion and cell polarity, and gain some characteristics of mesenchymal cell, such as motility, invasion, and anti-apoptosis. EMT changes the type of tumor cells,

improves the ability to degrade the matrix, and weakens cell-to-cell binding.[29] Therefore, transformed tumor cells are the main cause of tumor death, have greater metastatic and invasive abilities. Hence, prevention and treatment of metastasis and improvement of clinical prognosis are key. One of the hallmarks of EMT is the downregulation or even loss of E-cadherin expression, a feature that promotes tumor invasion and metastatic capacity. TGF-β1 and β-catenin signaling pathways can activate snail, inhibit E-cadherin, induce EMT and promote cell migration.[30] Vimentin is an important type III intermediate filament protein. Together with other cytoskeletal components such as microfilaments and microtubules, it plays an important role in dynamic processes such as the support, attachment, migration, and signaling of cellular structures.[31] As a result, Vimentin is considered as a typical molecular marker of EMT.[32] In our study, we found that EMT was also present in CAG. Wound healing assay showed that MNNG-induced GES-1 cells migration was enhanced. In contrast, XLHZ could increase the expression of E-cadherin and decrease the expression of TGF-β1, β-catenin and Vimentin, inhibit EMT and cell migration in MNNG-induced GES-1 cells. Uncontrolled proliferation and anti-apoptosis are the remarkable characteristics of tumor cells, which are the basis of the occurrence and development of tumor diseases. The imbalance of cell cycle regulation is an important cause of tumor cell proliferation. Therefore, regulating cell cycle, inhibiting proliferation and promoting apoptosis are important ways of tumor treatment.[33] Cells are regulated at different checkpoints through the interaction of various cyclin proteins with their cyclin-dependent kinases (CDKS) to form active complexes. The process of each checkpoint is completed accurately before proceeding to the next phase of the cell cycle.[34] Among them, CDK1, 2, 4, and 6 play major roles in cell cycle progression. This process is highly disturbed in cancer cells.[35] Previous study has shown that miR-33a could arrest gastric cancer cells in G1 phase and inhibit the proliferation of gastric cancer cells by down-regulating CDK6, cyclin D1 and Recombinant Pim-1 Oncogene.[36] Apoptosis, also known as programmed death, is a homeostatic mechanism that controls cell number and refers to the autonomous and orderly death of cells controlled by genes. Abnormal apoptosis can cause a variety of diseases, such as excessive apoptosis can induce Alzheimer's disease, and too little apoptosis can induce tumors.[37] Wei *et al* [38] found that miR-15b-3p could inhibit cell apoptosis and promote the malignant transformation of gastric cancer through dynein light chain Tctex-type 1/Caspase-3/Caspase-9 signaling pathway. Our study showed that XLHZ could arrest cells in G0/G1 and G2/M phases, inhibit cell proliferation, and promote apoptosis. These results suggest that XLHZ may play an important role in the inhibition of DAN synthesis, thus blocking the development of CAG into GC.

In conclusion, the results show that XLHZ affects the biological functions of CAG cells, such as proliferation, migration and invasion, apoptosis and tumor stem cell characteristics, by altering miRNA expression profiles and regulating downstream target genes, thus affecting the tumor micro-environment and improving EMT, which in turn affects the progression of CAG, and *in vitro* experiments also validate this aspect of XLHZ function. This study provides a new idea for XLHZ to treat CAG. However, due to the limitation of sample size, the miRNA study may be biased and we will conduct a study with larger samples when the opportunity arises. In the future, we will also explore in depth the mechanistic relationship between specific components of traditional Chinese medicine and differentially expressed miRNAs, hoping to provide potential biological targets for the treatment of CAG to GC.

5. SUPPORTING INFORMATION

Supporting data to this article can be found online at http://journaltcm.cn.

6. REFERENCES

1. Piscione M, Mazzone M, Di Marcantonio MC, et al. Eradication of Helicobacter pylori and gastric cancer: a controversial relationship. Front Microbiol 2021; 12: 630852.
2. Ohata H, Kitauchi S, Yoshimura N, et al. Progression of chronic atrophic gastritis associated with Helicobacter pylori infection increases risk of gastric cancer. Int J Cancer 2004; 109: 138-43.
3. Correa P. Human gastric carcinogenesis: a multistep and multifactorial process--First American Cancer Society Award Lecture on Cancer Epidemiology and Prevention. Cancer Res 1992; 52: 6735-40.
4. Compare D, Rocco A, Nardone G. Risk factors In gastric cancer. Eur Rev Med Pharmacol Sci 2010; 14: 302-8.
5. Taniguchi K, Karin M. NF-κB, inflammation, immunity and cancer: coming of age. Nat Rev Immunol 2018; 18: 309-24.
6. Kaltschmidt B, Greiner JFW, Kadhim HM, et al. Subunit-specific role of NF-κB in cancer. Biomedicines 2018; 6: 44.
7. Mayer RJ, Venook AP, Schilsky RL. Progress against GI cancer during the american society of clinical oncology's first 50 years. J Clin Oncol 2014; 32: 1521-30.
8. Rodriguez-Castro KI, Franceschi M, Noto A, et al. Clinical manifestations of chronic atrophic gastritis. Acta Biomed 2018; 89: 88-92.
9. Sharma PK, Suri TM, Venigalla PM, et al. Atrophic gastritis with high prevalence of Helicobacter pylori is a predominant feature in patients with dyspepsia in a high altitude area. Trop Gastroenterol 2014; 35: 246-51.
10. Gu Z, Jia Q, Cong J, et al. Efficacy and safety of Elian Granules in treating chronic atrophic gastritis: study protocol for a randomized, double-blind, placebo-controlled, multicenter clinical trial. Trials 2022; 23: 437.
11. Ou J, Wang L. Efficacy of self-made Hewei decoction for chronic atrophic gastritis and its effect on gastrin and pepsinogen expression levels. Contrast Media Mol Imaging 2022; 2022: 1092695.
12. Yang T, Wang R, Zhang J, et al. Mechanism of berberine in treating Helicobacter pylori induced chronic atrophic gastritis through IRF8-IFN-γ signaling axis suppressing. Life Sci 2020; 248: 117456.
13. Tong Y, Wang R, Liu X, et al. Zuojin pill ameliorates chronic atrophic gastritis induced by MNNG through TGF-β1/PI3K/Akt axis. J Ethnopharmacol 2021; 271: 113893.
14. Wang J, Gao YX, Ma HY, et al. Mechanism of Xianglian Huazhuo prescription against chronic atrophic gastritis based on network pharmacology and experimental verification. Zhong Guo Shi Yan

Fang Ji Xue Za Zhi 2022; 28: 161-8.
15. Gao YX, Wang J, Ma HY, et al. Effects of Xianglian Huazhuo recipe on apoptosis signal pathway related factors in rats with chronic atrophic gastritis. Zhong Hua Zhong Yi Yao Za Zhi 2023; 38: 1050-7.
16. Wang J, Ma HY, Gao YX, et al. Protective effect of Huazhuo Jiedu recipe on chronicatrophic gastritis in rats. Zhong Guo Zhong Xi Yi Jie He Za Zhi 2022; 42: 348-54.
17. Hu ML, Xiong SW, Zhu SX, et al. MicroRNAs in gastric cancer: from bench to bedside. Neoplasma 2019; 66: 176-86.
18. Cheng J, Yang A, Cheng S, et al. Circulating miR-19a-3p and miR-483-5p as novel diagnostic biomarkers for the early diagnosis of gastric cancer. Med Sci Monit 2020; 26: e923444.
19. Feng X, Zhu M, Liao B, et al. Upregulation of miR-552 predicts unfavorable prognosis of gastric cancer and promotes the proliferation, migration, and invasion of gastric cancer cells. Oncol Res Treat 2020; 43: 103-11.
20. Xu J, Zhang Z, Chen Q, et al. miR-146b regulates cell proliferation and apoptosis in gastric cancer by targeting PTP1B. Dig Dis Sci 2020; 65: 457-63.
21. Nardone G, Rocco A, Compare D, et al. Is screening for and surveillance of atrophic gastritis advisable? Dig Dis 2007; 25: 214-7.
22. Zhou Y, Xu Q, Shang J. et al, Crocin inhibits the migration, invasion,and epithelial-mesenchymal transition of gastric cancer cells *via* miR-320/KLF5/HIF-lα signaling. J Cell Physiol 2019; 234: 17876-85.
23. Song M, Wang X, Luo Y, et al. Cantharidin suppresses gastric cancer cell migration/invasion by inhibiting the PI3K/Akt signaling pathway *via* CCAT1, Chem Biol Interact 2020; 317: 108939.
24. Liu ZM, Yang XL, Jiang F, et al. Matrine involves in theprogression of gastric cancer through inhibiting miR-93-Sp and upregulating the expression of target gene AHNAK. J Cell Biochem 2020; 121: 2467-77.
25. Tsukamoto H, Mizoshita T, Katano T, et al. Preventive effect of rebamipide on N-methyl-N'-nitro-N-nitrosoguanidine-induced gastric carcinogenesis in rats. Exp Toxicol Pathol 2015; 67: 271-7.
26. Si J, Zhou W, Wu J, et al. Establishment of an animal model of chronic atrophic gastritis and a study on the factors inducing atrophy. Chin Med J (Engl) 2001; 114: 1323-5.
27. Adams BD, Kasinski AL, Slack FJ. Aberrant regulation and function of microRNAs in cancer. Curr Biol 2014; 24: R762-76.
28. Seven M, Karatas OF, Duz MB, et al. The role of miRNAs in cancer: from pathogenesis to therapeutic implications. Future Oncol 2014; 10: 1027-48.
29. Seeneevassen L, Bessède E, Mégraud F, et al. Gastric cancer: advances in carcinogenesis research and new therapeutic strategies. Int J Mol Sci 2021; 22: 3418.
30. Usman S, Waseem NH, Nguyen TKN, et al. Vimentin is at the heart of epithelial mesenchymal transition (EMT) mediated metastasis. Cancers (Basel) 2021; 13: 4985.
31. Danielsson F, Peterson MK, Caldeira Araújo H, et al. Vimentin diversity in health and disease. Cells 2018; 7: 147.
32. Liu CY, Lin HH, Tang MJ, et al. Vimentin contributes to epithelial-mesenchymal transition cancer cell mechanics by mediating cytoskeletal organization and focal adhesion maturation. Oncotarget 2015; 6: 15966-83.
33. Wenzel ES, Singh ATK. Cell-cycle checkpoints and aneuploidy on the path to cancer. In Vivo 2018; 32: 1-5.
34. Khan M, Rasul A, Yi F, et al. Jaceosidin induces p53-dependent G2/M phase arrest in U87 glioblastoma cells. Asian Pac J Cancer Prev 2011; 12: 3235-8.
35. Icard P, Fournel L, Wu Z, et al. Interconnection between metabolism and cell cycle in cancer. Trends Biochem Sci 2019; 44: 490-501.
36. Wang Y, Zhou X, Shan B, et al. Downregulation of microRNA-33a promotes cyclin-dependent kinase 6, cyclin D1 and PIM1 expression and gastric cancer cell proliferation. Mol Med Rep 2015; 12: 6491-500.
37. Xu X, Lai Y, Hua ZC. Apoptosis and apoptotic body: disease message and therapeutic target potentials. Biosci Rep 2019; 39: BSR20180992.
38. Wei S, Peng L, Yang J, et al. Exosomal transfer of miR-15b-3p enhances tumorigenesis and malignant transformation through the DYNLT1/caspase-3/caspase-9 signaling pathway in gastric cancer. J Exp Clin Cancer Res 2020; 39: 32.